

Molecular junctions in the Coulomb blockade regime: rectification and nesting

Bo Song, Dmitry A. Ryndyk, and Gianaurelio Cuniberti
Institute for Theoretical Physics, University of Regensburg, D-93040 Germany
(Dated: November 7, 2006)

Quantum transport through single molecules is very sensitive to the strength of the molecule-electrode contact. Here, we investigate the behavior of a model molecular junction weakly coupled to external electrodes in the case where charging effects do play an important role (Coulomb blockade regime). As a minimal model, we consider a molecular junction with two spatially separated donor and acceptor sites. Depending on their mutual coupling to the electrodes, the resulting transport observables show well defined features such as rectification effects in the I - V characteristics and nesting of the stability diagrams. To be able to accomplish these results, we have developed a theory which allows to explore the charging regime via the nonequilibrium Green function formalism parallel to the widely used master equation technique. Our results, beyond their experimental relevance, offer a transparent framework for the systematic and modular inclusion of a richer physical phenomenology.

PACS numbers: 85.65.+h, 73.23.-b, 73.23.Hk, 85.30.Kk

I. INTRODUCTION

Single molecule electronics^{1,2,3} has been mostly investigated in the high temperature and strong contact to the electrode regime. The opposite limit of low temperature and weakly coupled molecular junctions pose a challenge to the currently available experimental techniques. Still the possibility to probe the spectroscopy of single molecule junctions via a lateral gate could offer new insights in the peculiar coupling of the electrical and mechanical degrees of freedom at the nanoscale. In order to be able to establish the transport mechanisms governing such molecular junctions in the Coulomb blockade (CB) regime, a technique which could tackle on one hand single electron charging effects and, on the other hand, the inclusion of the electron-vibron coupling is of extreme importance. The nonequilibrium Green function (NEGF) formalism has been recently employed to describe transport observables on the base of a density functional theory description of the electronic structure^{2,4,5,6,7,8,9,10} and model Hamiltonian approaches.^{11,12,13,14} The NEGF was applied to describe the influence of the vibron dynamics onto a molecular transistor in the strong coupling regime^{15,16} but it is typically substituted with master equation approaches when coming to the case of weak coupling to the electrodes. Our purpose is to study the problem of a two site donor/acceptor molecule in the CB regime within the NEGF as a first step to deal with the phenomenology of a rigid multilevel island. The nuclear dynamics (vibrations) always present in molecular junctions could be then modularly included in this theory. Our method developed in this paper can be calibrated on the well-studied double quantum dot problem¹⁷ and could be possibly integrated in density functional theory based approaches to molecular conductance.

Here, we apply our theory to the case of a two site energetically asymmetric molecular junction. In the case of serial coupling to the electrodes, this configuration consists, de facto, in a molecular rectifier (diode) as proposed

long time ago by Aviram and Ratner¹⁸ and recently experimentally realized.¹⁹ We show that the sequential tunneling regime, being a fundamental different regime from coherent transport, is compatible to the observed rectification features.¹⁹ The serial arrangement of a double site correlated molecule between two leads is possibly the simplest configuration. The most general case (see Fig. 1), which includes parallel pathways, shows in the sequential tunneling regime an interplay of correlated effect and interference eventually bringing to the phenomenon of a nesting of the stability diagrams due to possible different charging energies.

In this paper, we introduce a powerful *Ansatz* for the NEGF which is related both to the equation-of-motion (EOM) method and to the Dyson equation approach. From the knowledge of the Green function (GF) we then calculate the transport observables. Our results are of a particular interest in its own at a formal level. In the case of a single site junction (SSJ) with Coulomb interaction (Anderson impurity model), the *conductance* properties have been successfully studied by means of the EOM approach in the cases related to CB²⁰ and the Kondo effect.²¹ Later the same method was applied to some

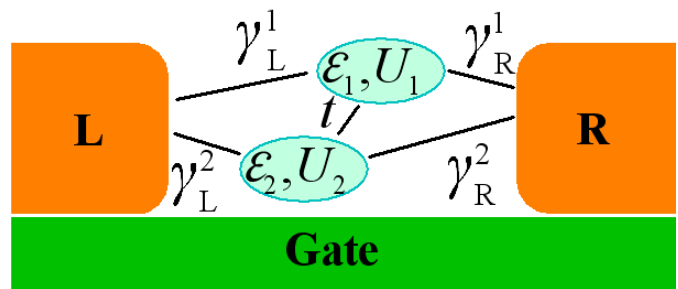


FIG. 1: (color) The general configuration of a double site junction. The levels $\epsilon_{1,2}$ with charging energies $U_{1,2}$ are connected via t and coupled to the electrodes via the linewidth injection rates γ_{α}^i .

two-site models.^{11,22,23} Multi-level systems were started to be considered only recently.^{24,25} Besides, there are some difficulties in building the lesser GF in the nonequilibrium case (at finite bias voltages) by means of the EOM method.^{26,27,28} Here, we develop a self-consistent nonequilibrium method for the GF of a single-site junction (SSJ) and of a double-site junctions (DSJ). The results of the EOM method could be calibrated with other available calculations, such as the master equation approach and the non-crossing approximation. This paper is organized as follows: after the derivation of the SSJ and the DSJ nonequilibrium results for the retarded and lesser GFs (Sec. II), we do show their effects on the transport observables (Sec. III).

II. SYSTEM AND METHOD

The goal of this paper is the determination of the transport observables for a minimal model of a molecular-junction in the CB regime, namely a double site correlated impurity Hamiltonian coupled to extended electrode states. For clarity, we first describe our method in the more familiar problem of a single site junction, which is the well-known Anderson impurity model.

A. Single site case

The Anderson impurity model is used to describe the Coulomb interaction on a single site:

$$H = H_D + \sum_{\alpha} (H_{\alpha} + H_{\alpha D}),$$

where

$$H_D = \sum_{\sigma} \epsilon_{\sigma} d_{\sigma}^{\dagger} d_{\sigma} + \frac{1}{2} U n_{\sigma} n_{\bar{\sigma}},$$

$$H_{\alpha} = \sum_{k,\sigma} \epsilon_{k,\sigma}^{\alpha} c_{\alpha,k,\sigma}^{\dagger} c_{\alpha,k,\sigma},$$

$$H_{\alpha D} = \sum_{k,\sigma} \left(V_{\alpha,k,\sigma} c_{\alpha,k,\sigma}^{\dagger} d_{\sigma} + V_{\alpha,k,\sigma}^{*} d_{\sigma}^{\dagger} c_{\alpha,k,\sigma} \right),$$

where d and c are the operators for electrons on the dot and on the left ($\alpha = L$) and the right ($\alpha = R$) lead, U is the Coulomb interaction parameter, ϵ_{σ} is the σ level of the quantum dot, while $\epsilon_{k,\sigma}^{\alpha}$ are σ level of lead α in k space, $\sigma = \uparrow, \downarrow$. With the help of the EOM and a truncation approximation, we can get a closed set of equations for the retarded and advanced GFs $G_{\sigma,\tau}^{r/a}$,

$$(\omega - \epsilon_{\sigma} - \Sigma_{\sigma}^{r/a}) G_{\sigma,\tau}^{r/a} = \delta_{\sigma,\tau} + U G_{\sigma,\tau}^{(2)r/a}, \quad (1a)$$

$$(\omega - \epsilon_{\sigma} - U - \Sigma_{\sigma}^{r/a}) G_{\sigma,\tau}^{(2)r/a} = \langle n_{\bar{\sigma}} \rangle \delta_{\sigma,\tau}, \quad (1b)$$

where $G_{\sigma,\tau}^{r/a} = \langle \langle d_{\sigma} | d_{\tau}^{\dagger} \rangle \rangle^{r/a}$, $G_{\sigma,\tau}^{(2)r/a} = \langle \langle n_{\bar{\sigma}} d_{\sigma} | d_{\tau}^{\dagger} \rangle \rangle^{r/a}$ and

$$\Sigma_{\sigma}^{r/a}(\omega) = \Sigma_{L,\sigma}^{r/a} + \Sigma_{R,\sigma}^{r/a} = \sum_{\alpha,k} \frac{|V_{\alpha,k,\sigma}|^2}{\omega - \epsilon_{k,\sigma}^{\alpha} \pm i0^{+}} \quad (2)$$

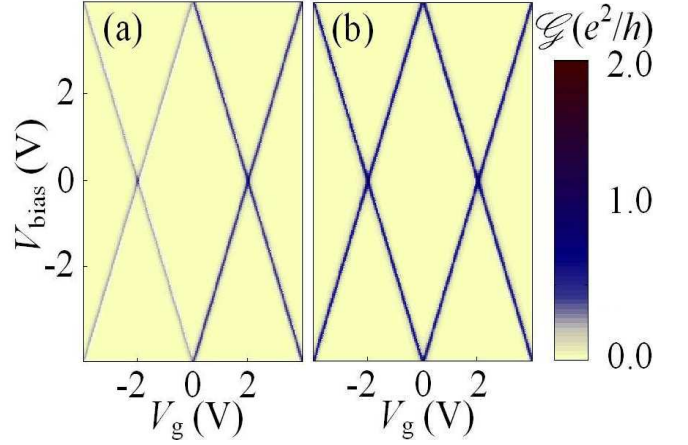


FIG. 2: (color) The stability diagram of a SSJ with $\epsilon_{\sigma} = 2.0$ eV, $U = 4.0$ eV, $\Gamma_L = \Gamma_R = 0.05$ eV. (a) The incorrect result obtained by means of the widely used formula in Eq. (9) for the lesser GF is not symmetric for levels ϵ_{σ} and $\epsilon_{\sigma} + U$. (b) Results obtained by means of our Ansatz in Eq. (7) shows correctly symmetric for levels ϵ_{σ} and $\epsilon_{\sigma} + U$.

are the electron self-energies.

1. Mapping on retarded Green functions: equilibrium case

There are two typical ways to calculate GFs. The first is by means of the Dyson equation and Feynman diagrams, the second is by means of the EOM.³⁰ For retarded GFs, from the EOM method, and with the help of Eqs. (1a) and (1b), we can get

$$\begin{aligned} G^r &= G_0^r + G_0^r U G^{(2)r} \\ &= G_0^r + G_0^r \Sigma^{EOM} G^{(1)r}, \end{aligned}$$

where G^r is single-particle GF matrix

$$G^r = \begin{pmatrix} G_{\uparrow,\uparrow}^r & G_{\uparrow,\downarrow}^r \\ G_{\downarrow,\uparrow}^r & G_{\downarrow,\downarrow}^r \end{pmatrix},$$

and $G_{\sigma,\tau}^{(1)r} = G_{\sigma,\tau}^{(2)r} / \langle n_{\bar{\sigma}} \rangle$. G_0^r describes the single-particle spectrum without Coulomb interaction, but including the effects from the electrodes. $\Sigma_{\sigma,\tau}^{EOM} = U \langle n_{\bar{\sigma}} \rangle$ is the Hartree-like self-energy of our model. Since there is only Coulomb interaction on the site with the levels ϵ_{σ} , the Fock-like self-energy is vanishing.

Alternatively, by means of the Dyson equation and the second-order truncation approximation, taking Hartree-like self-energies $\Sigma_{\sigma,\tau}^H = U \langle n_{\bar{\sigma}} \rangle$ ($= \Sigma_{\sigma,\tau}^{EOM}$), we can also get the retarded GFs as follows,³⁰

$$G^r = G_0^r + G_0^r \Sigma^H G_1^r, \quad (3)$$

where $G_1^r = G_0^r + G_0^r \Sigma^H G_0^r$ is the first-order truncation GF.

Within the level of the second-order truncation approximation, we see that there is a map between the EOM results and the Dyson results:

$$G^r = G_0^r + G_0^r \Sigma^H G^{(1)r} \quad \text{EOM,} \quad (4a)$$

$$\begin{array}{ccc} \updownarrow & & \updownarrow \\ G^r = G_0^r + G_0^r \Sigma^H G_1^r & \text{Dyson.} & (4b) \end{array}$$

Eqs. (4) prompts a way to include further many-particle effects into the Dyson equation, (Eq. (4b)), by replacing the *Dyson-first-order* retarded Green function G_1^r with the *EOM* $G^{(1)r}$. Then one obtains already the correct results to describe CB while keeping the Hartree-like self-energy.

2. Mapping on contour Green functions: nonequilibrium case

Introducing now the contour GF \check{G} , we can get the Dyson equation as follows,^{29,31,32,33}

$$\check{G} = \check{G}_0 + \check{G}_0 \check{\Sigma} \check{G}, \quad (5)$$

where $\check{\Sigma}$ is the self-energy matrix.²⁹

According to the approximation for the retarded GF in Eq. (3), we take the second-order truncation on Eq. (5), and then get

$$\check{G} = \check{G}_0 + \check{G}_0 \check{\Sigma}^H \check{G}_1,$$

where $\check{G}_1 = \check{G}_0 + \check{G}_0 \check{\Sigma}^H \check{G}_0$ is the first-order contour GF, and \check{G}_0 has already included the lead effects.

Similar to the mapping in Eq. (4), we perform an *Ansatz* consisting in substituting the *Dyson-first-order* $G_1^{r/a/<}$ with the *EOM* one $G^{(1)r/a/<}$ to consider more many-particle correlations, while the *EOM* self-energy is used for the *Dyson* equation for consistency:

$$\begin{array}{ccc} \check{G} = \check{G}_0 + \check{G}_0 \check{\Sigma}^H \check{G}_1 & \text{Dyson,} & \\ \updownarrow & & \up \\ \check{G} & & \check{G}^{(1)} \quad \text{EOM.} \end{array} \quad (6)$$

Then, using the Langreth theorem,²⁹ we get the lesser GF,

$$\begin{aligned} G^< &= G_0^< + G_0^r \Sigma^{H,r} G^{(1)<} + G_0^< \Sigma^{H,a} G^{(1)a} \\ &= G_0^< + G_0^r U G^{(2)<} + G_0^< U G^{(2)a} \end{aligned} \quad (7)$$

where $G_0^{r/a/<}$ are GFs for $U = 0$, *but* including the lead effects, *i.e.*

$$\begin{aligned} G_0^< &= g_0^< + g_0^r \Sigma^< G_0^a + g_0^< \Sigma^a G_0^a + g_0^r \Sigma^r G_0^<, \\ G_0^{r/a} &= g_0^{r/a} + g_0^{r/a} \Sigma^{r/a} G^{r/a}, \end{aligned}$$

with $g_0^{r/a/<}$ the free electron GF, and

$$\Sigma^{r/a/<} = \begin{pmatrix} \Sigma_{\uparrow}^{r/a/<} & 0 \\ 0 & \Sigma_{\downarrow}^{r/a/<} \end{pmatrix},$$

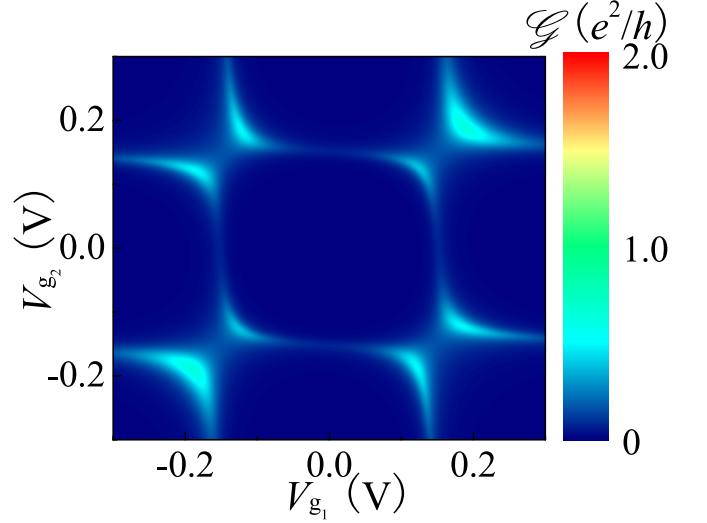


FIG. 3: (color) The stability diagram of serial DSJ with $\epsilon_{1,\sigma} = \epsilon_{2,\sigma} = -0.15$ eV, $U_1 = U_2 = 0.3$ eV, $t = 0.05$ eV, $\gamma_L^1 = \gamma_R^2 = 0.02$ eV, $\gamma_L^2 = \gamma_R^1 = 0$, $V_{\text{bias}} = 0.005V$.

$\Sigma_{\sigma}^< = i \sum_{\alpha} \Gamma_{\alpha} f_{\alpha}(\omega)$, and $\Gamma_{\alpha} = i(\Sigma_{\alpha}^r - \Sigma_{\alpha}^a)$, $f_{\alpha}(\omega) = f(\omega - \mu_{\alpha})$, f is the equilibrium Fermi function and μ_{α} is the electro-chemical potential in lead α ; $\Sigma_{\alpha}^{r/a}$ are the retarded/advanced electron self-energies from Eq. (2) and $G_{\sigma,\tau}^{(1)r/a/<} = G_{\sigma,\tau}^{(2)r/a/<} / \langle n_{\bar{\sigma}} \rangle$. Performing the same *Ansatz* on the double-particle GF, from Eq. (1b) we can get

$$G^{(2)<} = G^{(2)r} \Sigma^{(2)<} G^{(2)a}, \quad (8)$$

with $\Sigma_{\sigma}^{(2)<} = \Sigma_{\sigma}^< / \langle n_{\bar{\sigma}} \rangle$.

The lesser GFs in Eq. (7) can also be obtained directly from the general formula²⁹

$$\check{G}^<(\omega) = \check{G}_0^< + \check{G}_0^r \check{\Sigma}^r \check{G}^< + \check{G}_0^r \check{\Sigma}^< \check{G}^a + \check{G}_0^< \check{\Sigma}^a \check{G}^a,$$

with the help of the *Ansatz* in Eq. (6). It should be noted that Eq. (7) is very different from the lesser GF formula,

$$G^< = G^r \Sigma^< G^a, \quad (9)$$

which is widely used for both first-principle^{4,9,34} and model Hamiltonian calculations.¹¹ It should be noted that the self-energy $\Sigma^<$ in Eq. (9) contains *only* contributions from the electrodes.

The numerical calculation results of conductance dependence on the bias and gate voltages by the two different NEGF Eqs. (7) and (9) are shown in Fig. 2. As we can see in the left panel, the adoption of Eq. (9) results in incorrectly symmetry-breaking in the gate potential. This wrong behavior is corrected in the right panel where Eq. (7) has been used.

B. Double site case

We now investigate the DSJ system with Coulomb interaction on each dot site. The Hamiltonian is expressed as follows,

$$H = H_D + H_t + \sum_{\alpha} (H_{\alpha} + H_{\alpha D}),$$

where

$$\begin{aligned} H_D &= \sum_{i,\sigma} \epsilon_{i,\sigma} d_{i,\sigma}^{\dagger} d_{i,\sigma} + \frac{U_i}{2} n_{i,\sigma} n_{i,\bar{\sigma}}, \\ H_t &= \sum_{i \neq j, \sigma} \frac{t}{2} (d_{i,\sigma}^{\dagger} d_{j,\sigma} + d_{j,\sigma}^{\dagger} d_{i,\sigma}), \\ H_{\alpha,\sigma} &= \sum_{k,\sigma} \epsilon_{k,\sigma}^{(\alpha)} c_{\alpha,k,\sigma}^{\dagger} c_{\alpha,k,\sigma}, \\ H_{\alpha D,\sigma} &= \sum_{k,\sigma} \left(V_{\alpha,k,\sigma} c_{\alpha,k,\sigma}^{\dagger} d_{i,\sigma} + V_{\alpha,k,\sigma}^* d_{i,\sigma}^{\dagger} c_{\alpha,k,\sigma} \right), \end{aligned}$$

with $i, j = 1, 2$ indicate the dot site, t is the constant for electron hopping between different sites.

With the help of the EOM, and by means of the truncation approximation on the double-particle GFs, we obtain the closed form for the retarded GFs as follows

$$\begin{aligned} (\omega - \epsilon_{i,\sigma} - \Sigma_{i,\sigma}^r) G_{i,\sigma;j,\tau}^{(U,t)r} & \\ = \delta_{i,j} \delta_{\sigma,\tau} + U_i G_{i,\sigma;j,\tau}^{(2)(U,t)r} + t G_{i,\sigma;j,\tau}^{(U,t)r}, & \quad (10a) \end{aligned}$$

$$\begin{aligned} (\omega - \epsilon_{i,\sigma} - U_i - \Sigma_{i,\sigma}^r) G_{i,\sigma;j,\tau}^{(2)(U,t)r} & \\ = \langle n_{i,\bar{\sigma}} \rangle \delta_{i,j} \delta_{\sigma,\tau} + t n_{i,\sigma} G_{i,\sigma;j,\tau}^{(U,t)r}, & \quad (10b) \end{aligned}$$

where the DSJ retarded GFs are defined as $G_{i,j;\sigma,\tau}^{(U,t)r} = \langle\langle d_{i,\sigma} | d_{j,\tau}^{\dagger} \rangle\rangle^r$, $G_{i,j;\sigma,\tau}^{(2)(U,t)r} = \langle\langle n_{i,\bar{\sigma}} d_{i,\sigma} | d_{j,\tau}^{\dagger} \rangle\rangle^r$. \bar{i} means 'NOT i ', and $\Sigma_{i,\sigma}^r$ are the electron self-energy from leads. From Eqs. (10a), (10b) and performing the same *Ansatz* as in the case of SSJ, we can obtain the DSJ lesser GFs with Coulomb-interaction effects as follows,

$$\begin{aligned} G^{(U,t)<}(\omega) &= (1 + G^{(U,t)r} \Sigma_t^r) G^{(U)<} \\ &\cdot (1 + \Sigma_t^a G^{(U,t)a} + G^{(U,t)r} \Sigma_t^< G^{(U,t)a}), \quad (11) \end{aligned}$$

with

$$\Sigma_t^r = \Sigma_t^a = \begin{pmatrix} 0 & t & 0 & 0 \\ t & 0 & 0 & 0 \\ 0 & 0 & 0 & t \\ 0 & 0 & t & 0 \end{pmatrix},$$

and $\Sigma_t^< = 0$. $G^{(U)<}$ is the DSJ lesser GF with the same form as Eq. (7), but taking

$$U = \begin{pmatrix} U_1 & 0 & 0 & 0 \\ 0 & U_2 & 0 & 0 \\ 0 & 0 & U_1 & 0 \\ 0 & 0 & 0 & U_2 \end{pmatrix}, \quad \Gamma_{\alpha} = \begin{pmatrix} \gamma_{\alpha}^1 & 0 & 0 & 0 \\ 0 & \gamma_{\alpha}^2 & 0 & 0 \\ 0 & 0 & \gamma_{\alpha}^1 & 0 \\ 0 & 0 & 0 & \gamma_{\alpha}^2 \end{pmatrix},$$

where γ_{α}^i indicates the line width function of lead α to site i , and U_i is the charging energy at site i . $G^{r/a}$ and $G^{(2)r/a}$ are the GF matrix from Eqs. (10a) and (10b). Here, in order to distinguish different GFs, we introduce the subscript '(U, t)' for the one with both Coulomb interaction U and inter-site hopping t , while '(U)' for the one only with Coulomb interaction.

For our models, the lesser GFs in Eq. (7), (8) and (11), which are obtained with help of our *Ansatz*, can also be obtained by the EOM NEGF formula in Eq. (A2) or in Ref. 26 within the same truncation approximation.

III. TRANSPORT OBSERVABLES FOR THE DOUBLE SITE JUNCTION

The current can be generally written as³⁵

$$\begin{aligned} J &= \frac{ie}{2\hbar} \int \frac{d\epsilon}{2\pi} \text{Tr}\{(\Gamma_L - \Gamma_R) G^{(U,t)<} \\ &+ [f_L(\omega)\Gamma_L - f_R(\omega)\Gamma_R](G^{(U,t)r} - G^{(U,t)a})\}, \end{aligned}$$

where the lesser GF is given by Eq. (11). The differential conductance is defined as

$$\mathcal{G} = \frac{\partial J}{\partial V_{\text{bias}}},$$

where the bias voltage is defined as $V_{\text{bias}} = (\mu_R - \mu_L)/e$.

A. Serial configuration

By taking $\gamma_L^2 = \gamma_R^1 = 0$, we obtain a serial DSJ, which could describe the kind of molecular quantum dot junctions like the ones in Ref. 19. First, at small bias voltages, the conductance with the two gate voltages V_{g_1} and V_{g_2} was calculated, and the relative stability diagram was obtained as shown in Fig. 3. Because of the double degeneracy (spin-up and spin-down) considered for each site and electrons hopping between the dots, there are eight resonance-tunnelling regions. This result is consistent with the master-equation approach.¹⁷

Further, we studied the nonequilibrium current for large bias-voltages (Fig. 4). Because $\epsilon_{1,\sigma}$ and $\epsilon_{2,\sigma}$ are taken as asymmetric, for the case without Coulomb interaction, the I - V curve is asymmetric for $\pm V_{\text{bias}}$, and there are one step and one maximum for the current. The step contributes to one peak for the conductance. When we introduce the Coulomb interaction to the system, the one conductance peak is split into several: two peaks, one pseudo-peak and one dip, while the current maximum comes to be double split (see Fig. 4). This process can be understood by the help of Fig. 5. At zero bias-voltage, $\epsilon_{2,\sigma}$ is occupied and $\epsilon_{1,\sigma}$ is empty. a) By adding a bias voltage, the Fermi window is opened. The level $\epsilon_{2,\sigma} + U$ is first resonant with the edge of the window. It will contribute the first peak for conductance. b) By

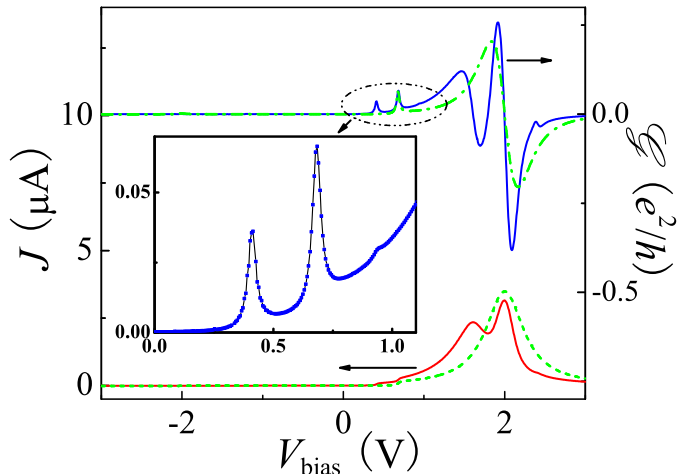


FIG. 4: (color) Current and conductance vs. bias-voltage of a DSJ far from equilibrium with parameters $\epsilon_{1,\sigma} = 0.5$ eV, $\epsilon_{2,\sigma} = -0.5$ eV, $U_1 = U_2 = U = 0.2$ eV, $t = 0.07$ eV, $\gamma_L^1 = \gamma_R^2 = 0.03$ eV, $V_{g_2} = -V_{g_1} = V_{\text{bias}}/4$ and $V_R = -V_L = V_{\text{bias}}/2$. The red curve represents the current, while the blue the conductance. The inset is the blow-up for the conductance peak split. The dash and dot-dash curves are for current and conductance with $U = 0$, respectively.

opening the window further, the levels $\epsilon_{2,\sigma}$ and $\epsilon_{1,\sigma}$ come into the window resulting in the second peak. c) When the level $\epsilon_{1,\sigma} + U$ comes in, only a pseudo-peak appears. This is because there is only a little possibility for electrons to occupy the level $\epsilon_{1,\sigma}$ under positive bias voltage. d) Levels $\epsilon_{2,\sigma} + U$ and $\epsilon_{1,\sigma}$ meet, which results in electron resonant-tunnelling and leads to the first maximum of the current. Then a new level $\epsilon_{1,\sigma} + U$ appears over the occupied $\epsilon_{1,\sigma}$ for charge effects. e) In Fig. 4(e), the meeting of $\epsilon_{2,\sigma}$ and $\epsilon_{1,\sigma}$ results in electron resonant tunnelling. It means that $\epsilon_{1,\sigma}$ will be occupied, which leads to the appearance of a new level $\epsilon_{1,\sigma} + U$. Then $\epsilon_{2,\sigma} + U$ meets $\epsilon_{1,\sigma} + U$ and another resonant tunnelling channel is opened for electrons. The two channels result in the second current maximum. f) Fig. 4(f) shows that the level $\epsilon_{1,\sigma} + U$ disappears if the level $\epsilon_{1,\sigma}$ is empty. This means that a dip appears in the conductance. It should be noted that the characteristics of serial DSJ in Fig. 4 have showed some reasonable similarities to experiments of a single-molecule diode.¹⁹

B. Parallel configuration

If on the other hand, the two sites are symmetrically connected to the electrodes, possibly with a small interdot hopping, but with different charging energies U_1 and U_2 , then the stability diagram would show some nesting characteristics (Fig. 6).

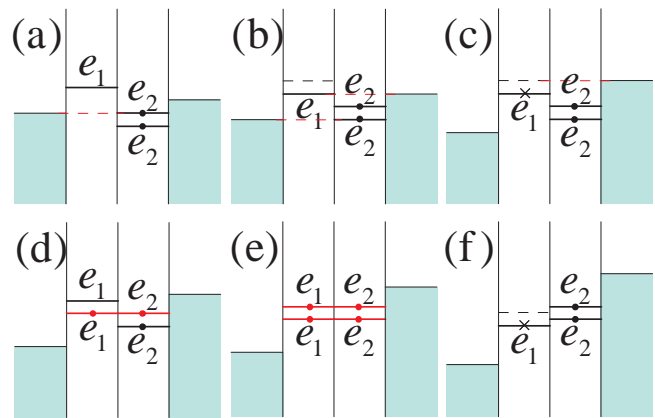


FIG. 5: (color) The processes involved in the transport characteristics in figure 4. $e_1 \equiv \epsilon_{1,\sigma}$, $e_2 \equiv \epsilon_{2,\sigma}$, $e_1^* \equiv \epsilon_{1,\sigma} + U$, $e_2^* \equiv \epsilon_{2,\sigma} + U$. The red line indicates electron resonant-tunnelling. a) The first conductance peak. b) The second conductance peak. c) The pseudo-peak of conductance. d) The first current maximum, and the red line indicates resonant tunnelling of electrons. e) The second current maximum for electron resonant tunnelling. f) The dip of conductance.

The physics of the thin lines in the figure can be understood by the help of charging effects. For simplicity, here we would ignore the site index i . In the region of large positive gate voltage at zero bias voltage, ϵ_{\uparrow} and ϵ_{\downarrow} are all empty, which means that the two levels are degenerate. Therefore adding a bias voltage, first, there will be two channels (ϵ_{\uparrow} and ϵ_{\downarrow}) opened for current (thick lines). After then, one level ϵ_{σ} (spin-up or spin-down) is occupied, while the other obtains a shift for Coulomb interaction: $\epsilon_{\bar{\sigma}} \rightarrow \epsilon_{\bar{\sigma}} + U$. Therefore, when the bias voltage is further increased to make the Fermi-window boundary meeting level $\epsilon_{\bar{\sigma}} + U$, only one channel is opened for the current, which results in the thin lines in Fig. 6. The similar case appears in the region of large negative gate voltages.

IV. CONCLUSIONS

In this paper, we introduced a powerful *Ansatz* for the lesser Green function, which is consistent with both the Dyson-equation approach and the equation-of-motion approach. By using this *Ansatz* together with the standard equation-of-motion technique for the retarded and advanced Green functions, we obtained the NEGF for both the single and the double site junctions in the Coulomb blockade regime *at finite voltages* and calculated the transport observables. The method can be applied to describe self-consistently transport through single molecules with strong Coulomb interaction and arbitrary coupling to the leads.

To test our method, we analyzed the CB stability diagram for a SSJ and a DSJ. Our results are all consistent with the results of experiments and the master-equation approach. We showed, that the improved lesser Green

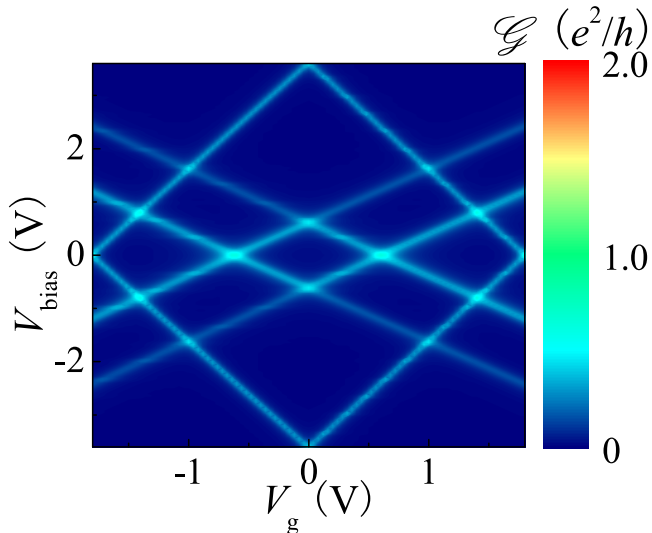


FIG. 6: (color) Nested stability diagram of a parallel DSJ with parameters $\epsilon_{1,\sigma} = -1.8$ eV, $\epsilon_{2,\sigma} = -0.3$ eV, $U_1 = 3.6$ eV, $U_2 = 0.6$ eV $t = 0.001$ eV, $\gamma_L^1 = \gamma_R^1 = 0.04$ eV, $\gamma_L^2 = \gamma_R^2 = 0.05$ eV, $V_{g_2} = V_{g_1}/2 = V_g/2$ and $V_R = -V_L = V_{\text{bias}}/2$.

function gives better results for weak molecule-to-contact couplings, where a comparison with the master equation approach is possible.

For the serial configuration of a DSJ, such as a donor/acceptor rectifier, the I - V curves maintain diode-like behavior, as it can be already inferred by coherent transport calculations.³⁶ Besides, we predict that as a result of the charging effects, one conductance peak will be split into three peaks and one dip, and one current maximum into two. For a DSJ parallel configuration, due to different charging energies on the two dot sites, the stability diagrams show peculiar nesting characteristics. In both cases, we present the results of numerical calculations as well as the simple qualitative picture of physical processes.

We believe, that the results presented here, beyond their experimental relevance, might be the transparent base for a systematic and modular inclusion of a richer physical phenomenology. Work is currently in progress to include the electron-vibron interactions to this theory.

V. ACKNOWLEDGMENTS

We acknowledge fruitful discussions with Rafael Gutierrez and Florian Pump. This work was funded by the Volkswagen Foundation under grant No. I/78 340, by the Deutsche Forschungsgemeinschaft within the Priority Program SPP 1243, and the trilateral project CU 44/3-2. Support from the Vielberth Foundation is also gratefully acknowledged.

APPENDIX A: DERIVATION OF THE EOM LESSER GREEN FUNCTION

From the view of perturbation theory, our Hamiltonian can be generally written as $H = H_0 + H_1$, where H_1 is the perturbation term to the solved H_0 . The contour-ordered GF is defined by means of the Schwinger-Keldysh time contour

$$\langle\langle A(\tau_1); B(\tau_2) \rangle\rangle^C = -i \langle T_C \{ A(\tau_1) B(\tau_2) \} \rangle, \quad (\text{A1})$$

where $A(\tau_1)$ and $B(\tau_2)$ are Heisenberg operators, defined along the contour C . Taking the time derivative, we obtain the EOM as,

$$i \frac{\partial}{\partial \tau_1} \langle\langle A(\tau_1); B(\tau_2) \rangle\rangle^C = \delta^C(\tau_1 - \tau_2) \langle [A(\tau_1), B(\tau_2)]_{\pm} \rangle + \langle\langle [A(\tau_1), H_1]; B(\tau_2) \rangle\rangle^C.$$

Using the free particle solution $g^C(\tau_1 - \tau_2)$, we can rewrite the time-dependent solution as

$$\langle\langle A(\tau_1); B(\tau_2) \rangle\rangle^C = g^C(\tau_1 - \tau_2) \langle [A(\tau_1), B(\tau_2)]_{\pm} \rangle + \int g^C(\tau_1 - \tau') \langle\langle [A(\tau'), H_1]; B(\tau_2) \rangle\rangle^C d\tau'.$$

Now applying the Langreth theorem and transforming in the spectral space, we get

$$\langle\langle A|B \rangle\rangle_{\omega}^< = g^<(\omega) \langle [A, B]_{\pm} \rangle + g(\omega)^r \langle\langle [A, H_1], B \rangle\rangle_{\omega}^< + g(\omega)^< \langle\langle [A, H_1], B \rangle\rangle_{\omega}^a. \quad (\text{A2})$$

¹ C. Joachim, J. K. Gimzewski, and A. Aviram, Nature (London) **408**, 541 (2000).

² G. Cuniberti, G. Fagas, and K. Richter, eds., vol. 680 of *Lecture Notes in Physics* (Springer, Berlin, 2005), ISBN 3-540-27994-6.

³ A. Nitzan and M. A. Ratner, Science **300**, 1384 (2003).

⁴ M. Brandbyge, J.-L. Mozos, P. Ordejón, J. Taylor, and

K. Stokbro, Phys. Rev. B **65**, 165401 (2002).

⁵ J. Taylor, M. Brandbyge, and K. Stokbro, Phys. Rev. B **68**, 121101 (2003).

⁶ T. Frauenheim, G. Seifert, M. Elstner, Z. Hajnal, G. Jungnickel, D. Porezag, S. Suhai, and R. Scholz, Phys. Stat. Sol. (b) **217**, 41 (2000).

⁷ A. D. Carlo, M. Gheorghie, P. Lugli, M. Sternberg,

- G. Seifert, and T. Frauenheim, *Physica B* **314**, 86 (2002).
- ⁸ T. Frauenheim, G. Seifert, M. Elstner, T. Niehaus, C. K. M. Amkreutz, M. Sternberg, Z. Hajnal, A. D. Carlo, and S. Suhai, *J. Phys.-Condens. Matter* **14**, 3015 (2002).
- ⁹ A. R. Rocha, V. M. Garcia-Suarez, S. Bailey, C. Lambert, J. Ferrer, and S. Sanvito, *Phys. Rev. B* **73**, 085414 (2006).
- ¹⁰ M. Albrecht, B. Song, and A. Schnurpfeil, *J. Appl. Phys.* **100**, 013702 (2006).
- ¹¹ P. Pals and A. Mackinnon, *J. Phys.-Condens. Matter* **8**, 5401 (1996).
- ¹² M. Galperin and A. Nitzan, *Ann. N.Y. Acad. Sci.* **1006**, 48 (2003).
- ¹³ M. Galperin, A. Nitzan, and M. A. Ratner, *Phys. Rev. Lett.* **96**, 166803 (2006).
- ¹⁴ A. A. Yanik, G. Klimeck, and S. Datta (2006), [cond-mat/0605037](#).
- ¹⁵ D. A. Ryndyk and J. Keller, *Phys. Rev. B* **71**, 073305 (2005).
- ¹⁶ D. A. Ryndyk, M. Hartung, and G. Cuniberti, *Phys. Rev. B* **73**, 045420 (2006).
- ¹⁷ W. G. van der Wiel, S. D. Franceschi, J. M. Elzerman, T. Fujisawa, S. Tarucha, and L. P. Kouwenhoven, *Rev. Mod. Phys.* **75**, 1 (2003).
- ¹⁸ A. Aviram and M. A. Ratner, *Chem. Phys. Lett.* **29**, 277 (1974).
- ¹⁹ M. Elbing, R. Ochs, M. Koentopp, M. Fischer, C. von Hanisch, F. Weigend, F. Evers, H. B. Weber, and M. Mayor, *Proc. Natl. Acad. Sci. USA* **102**, 8815 (2005).
- ²⁰ Y. Meir, N. S. Wingreen, and P. A. Lee, *Phys. Rev. Lett.* **66**, 3048 (1991).
- ²¹ Y. Meir, N. S. Wingreen, and P. A. Lee, *Phys. Rev. Lett.* **70**, 2601 (1991).
- ²² C. Niu, L.-J. Liu, and T.-H. Lin, *Phys. Rev. B* **51**, 5130 (1995).
- ²³ S. Lamba and S. K. Joshi, *Phys. Rev. B* **62**, 1580 (2000).
- ²⁴ J. J. Palacios, L. Liu, and D. Yoshioka, *Phys. Rev. B* **55**, 15735 (1997).
- ²⁵ L. Yi and J.-S. Wang, *Phys. Rev. B* **66**, 085105 (2002).
- ²⁶ C. Niu, D. L. Lin, and T.-H. Lin, *J. Phys.-Condens. Matter* **11**, 1511 (1999).
- ²⁷ R. Swirkowicz, J. Barnas, and M. Wilczynski, *Phys. Rev. B* **68**, 195318 (2003).
- ²⁸ B. R. Bulka and T. Kostyrko, *Phys. Rev. B* **70**, 205333 (2004).
- ²⁹ H. Haug and A.-P. Jauho, *Quantum Kinetics in Transport and Optics of Semiconductors* (Springer, Berlin, 1996).
- ³⁰ G. D. Mahan, *Many-Particle Physics* (Plenum Press, New York, 1990), 2nd ed.
- ³¹ L. Kadanoff and G. Baym, *Quantum Statistical Mechanics* (New York, Benjamin, 1962).
- ³² L. V. Keldysh, *Sov. Phys.-JETP* **20**, 1018 (1965).
- ³³ H. S. J. Rammer, *Rev. Mod. Phys.* **58**, 323 (1986).
- ³⁴ A. Pecchia and A. Di Carlo, *Reports on Progress in Physics* **67**, 1497 (2004).
- ³⁵ Y. Meir and N. S. Wingreen, *Phys. Rev. Lett.* **68**, 2512 (1992).
- ³⁶ F. Pump and G. Cuniberti (2006), [cond-mat/0611436](#).